

IX. Gépészeti Szakmakultúra Konferencia

IPMSM CSÚSZÓMÓD SZABÁLYOZÁSA A MUNKAPONTOK FIGYELEMBE VÉTELÉVEL

SLIDING MODE CONTROL OF IPMSM MACHINES ACCOUNTING FOR WORKING POINTS

Tóth-Katona Tamás*, Dr. Stumpf Péter**, Dr. Szabó Gergely***

ÖSSZEFOGLALÁS

A kutatás folyamán egy másodrendű forgó elektromechanikus rendszer hiszterézissel terhelt csúszómód szabályozás alapú megoldásait vizsgáljuk. Az elektromechanikus rendszer meghajtója egy IPMSM gép. A kutatás során az adaptív csúszófelület és adaptív elérési törvény metódusok kerültek kivizsgálásra, illetve kiértékelésre beállási idő, túllövés és beállási pontosság alapján.

ABSTRACT

In this paper sliding mode control methods of a second order electromechanical system was investigated. The driveline was loaded with a hysteresis profile and the drive of the system is an IPMSM. In this brief the adaptive sliding surface and adaptive reaching law methods were compared. The comparison is based on the respective settling time, settling precision and overshoot of the control strategy.

INTRODUCTION

The global trends in the electrification of drivelines show an upwards trend. More and more Internal Permanent Magnet Synchronous Machines (IPMSM) are used in electric or mild-hybrid vehicles. This is due to a number of positive attributes of IPMSMs, such as high efficiency, high power density and a wide-speed range operation. In many cases these systems have a number of uncertainties [1]. The uncertainties can vary from environmental hazards to driveline losses or changing parameters depending on the working point of the given driveline. To handle these uncertainties, many variable structure control (VSC) systems have been researched and many surveys and state-of-the-art papers were written in this field [2], [3]. Among the various VSC method Sliding Mode Control (SMC) is one of the most applied due to favorable characteristics such as robustness,

simplicity and possibility to reduce control system complexity by using hyperplanes.

The hyperplanes of the SMC controller are commonly sliding surfaces in the scientific literature. These sliding surfaces are defined in the systems m-dimensional phase plane which can be derived from the mathematical model given for the system. The sliding surfaces are reached according to a set of reaching laws, then the system is controlled to the desired state of the system via a control input. These phases of the control are called, reaching and sliding phase. Moreover, in modern electromechanical drivelines the control of the system is carried out with the help of digital electric circuit units (ECU) and microcontrollers. Therefore, discrete-time SMC (DSMC) controllers are more and more prevelant today [4]. In modern DSMC structures to enhance dynamic performance we may either introduce nonlinear sliding surfaces to achieve pre-defined finite settling time, resulting in terminal-DSMC [5]. Another way, is to attenuate the chattering by using high-order DSMC [6] or by using different switching based functions for the control law [7]. Nonetheless, further work is still needed regarding high dynamical electromechanical systems, where we account for hysteresis, input delay and input constraints. Therefore, in this paper we investigate the settling precision of a DSMC structure, where we account for control input constraints and hysteresis. The rest of the paper is organized as follows. In Sec.2 the theoretical background of the paper is established. In Sec.3 the designed discrete-time sliding mode controller is detailed with the selected reaching and sliding phase control laws. In Sec.0 the simulation results are presented. The simulations are carried out in Matlab/Simulink using discrete-time software (SW) modelling and continuous-time hardware modelling (HW). Finally, in section Sec.0 we conclude the paper, summarize the results and investigate improvement possibilities.

*** Instructor at at Budapest University of Technology and Economics , <u>szabo.gergely@vik.bme.hu</u>

-

^{*} PhD Student at Budapest University of Technology and Economics, <u>tamas.tothkatona@aut.bme.hu</u>

1. THEORETICAL BACKGROUND

In this section the theoretical background of the paper is provided, meaning the equations describing the system and the structure of the control loop.

1.1 Motion and machine equations of a second order electromechanical driveline.

In this paper the mechanical components of the electromechanical driveline are assumed to be modelled as a second order system, where reduced stiffness s and damping coefficient k are acting against the rotation of an axle's inertia Θ_m where the driving torque is hampered by a hysteresis characteristic $M_n(\mathbf{x})$.

Then, the motion equations of the electromechanical driveline can be written in a state space model as:

$$\begin{bmatrix} \dot{\varphi_{\rm m}} \\ \Omega_{\rm m} \end{bmatrix} = \underbrace{\begin{bmatrix} 0 & 1 \\ -s & -k \\ \overline{\Theta_{\rm m}} & \overline{\Theta_{\rm m}} \end{bmatrix}}_{\mathbf{A}} \begin{bmatrix} \varphi_{\rm m} \\ \Omega_{\rm m} \end{bmatrix} + \underbrace{\begin{bmatrix} 0 \\ 1 \\ \overline{\Theta_{\rm m}} \end{bmatrix}}_{\mathbf{b}} \underbrace{M_{\rm e}}_{\mathbf{u}} + \underbrace{\begin{bmatrix} 0 \\ -\frac{M_{\eta}}{\Theta_{\rm m}} \end{bmatrix}}_{\mathbf{d}} \tag{1}$$

where, **A** is the state matrix, **b** is the input matrix, **d** is the uncertainty vector, φ_m is the motor position, Ω_m is the motor speed, Θ_m is the electric drivelines reduced inertia, $M_{\eta}(\varphi_m)$ is a general state dependent hysteresis profile of the mechanical driveline, in this case linearly dependent on the motor position. Finally, M_e is the electric torque of the motor. In modern SMC control structures, the controlled state variables are to follow some reference trajectory. This is most done by introducing error functions given in equation (2)

$$\widetilde{\varphi}_{m} = \varphi_{m} - \varphi_{m}^{r}
\widetilde{\Omega}_{m} = \Omega_{m} - \Omega_{m}^{r}$$
(2)

where, $\varphi_{\rm m}^r$ and $\Omega_{\rm m}^r$ are reference motor position and speed.

To continue to adhere to the papers given in the following section, these error functions are used as the states of the state-space, this entwines the resultant state-space equations given in equation (3).

$$\dot{\mathbf{x}} = \mathbf{A}(\mathbf{x} - \mathbf{x}^r) + \mathbf{b}u + \mathbf{d} \tag{3}$$

Where,
$$\mathbf{x} = \begin{bmatrix} \widetilde{\varphi}_{\mathrm{m}} \\ \widetilde{\Omega}_{\mathrm{m}} \end{bmatrix}$$
 and $\mathbf{x}^r = \begin{bmatrix} \varphi_{\mathrm{m}}^r \\ \Omega_{\mathrm{m}}^r \end{bmatrix}$.

It is to be noted that, the difference based state space was made by subtracting the reference values and cannot be handled as initial condition of the state space equations, therefore, they are added to the state space model. The derived equivalent control law will be discussed in Sec.0. The control signal of the mechanical portion M_e of the electromechanical system is the electric torque of the

IPMSM within the system. The torque of an IPMSM can be calculated via motor parameters and the help of i_d and i_q current components as

$$M_{\rm e} = \frac{3}{2} n_{\rm P} i_{\rm q} (\Psi_{\rm PM} + \Delta L i_{\rm d}), \tag{4}$$

where $n_{\rm P}$ is the number of pole pairs in the IPMSM, $\Psi_{\rm PM}$ is the flux of the permanent magnet, $\Delta L = L_{\rm d} - L_{\rm q}$, where $L_{\rm d}$ and $L_{\rm q}$ are the d and q axis inductance of the machine. The voltage equation of an IPMSM where the iron losses are also considered can be written in dq-axis as [8]

$$v_d = R_s i_{d1} + L_d \frac{di_d}{dt} - \omega_1 L_q i_q$$

$$v_q = R_s i_{q1} + L_q \frac{di_q}{dt} + \omega_1 L_d i_d + \omega_1 \Psi_{PM}$$
(5)

where, $\omega_1 = n_P \Omega_m$ is the electric speed of the machine, R_s is the stator resistance, v_d and v_q are the direct and quadrature voltages. Furthermore, $i_{d1} = i_d + i_{di}$ and $i_{q1} = i_q + i_{qi}$ where i_{di} and i_{qi} are the d and q axis current through resistance R_i , expressing the iron loss of the machine [8]. Two constraint equations are given for the IPMSM. The voltage constraint given in the following equation (6).

$$\sqrt{v_{\rm d}^2 + v_{\rm q}^2} = V_1 \le V_{1,\rm max} = \frac{V_{\rm DC}}{\sqrt{3}}$$
 (6)

Where V_1 denotes the momentary amplitude of the stator voltage and V_{DC} is the DC bus voltage of the VSI. The current constraint equation given in the following equation (7).

$$\sqrt{i_{\rm d1}^2 + i_{\rm q1}^2} = I_1 \le I_{\rm max},\tag{7}$$

where I_1 denotes the momentary amplitude of the stator current and I_{max} is the maximum allowable current of the drive system.

1.2 Control Structure of the Driveline

On Fig.1 the control structure of the electric driveline can be seen. First, the reference position φ_m^r is passed to the sliding mode controller, which outputs the control input of the mechanical driveline, which is the reference torque. The reference torque of the IPMSM machine is calculated according to the machine equations given in equation (5) and based on the optimal searching-based reference current generation algorithm presented in the paper [8].

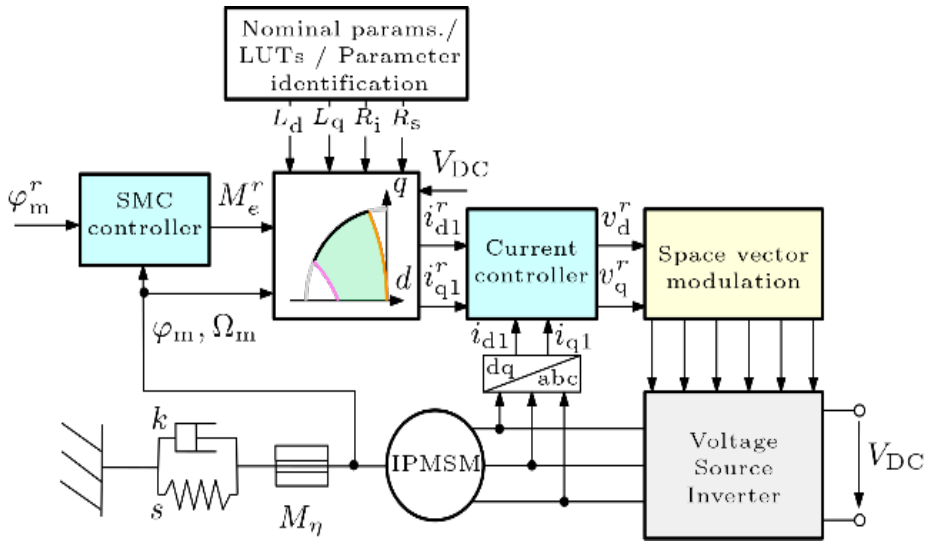


Fig. 1. Control structure of the electromechanical drive system.

The reference generating algorithm outputs the reference currents and passes them to the " Current Controller" block. The current controller was designed according to paper [9]. In the paper the closed loop current controller was designed using discrete time block-pole placement to define its dynamics. In case of a wide range of working points the motor parameters could vary, this can be handled with LUTs or parameter identification methods. The Space Vector Modulation (SVM) block implements the most commonly used so-called Min-Max modulation method and outputs the phase duties to the legs of the Voltage Source Inverter (VSI). The IPMSM model accounts for iron losses and copper losses. Finally, the SMC control of the electromechanical driveline is detailed. However as this is the main component of this article it is discussed separately in the following section.

2. SLIDING MODE CONTROLLER DESIGNS

In this section the designed sliding mode controller is described. Paper [10] proposed a sliding mode control where the sliding surface adapts according to the system state. It is suggested in that paper that all sliding surfaces should be stable and attracting the system states to the origin of the phase plane. Furthermore, a fuzzy logic and iterative cost function minimalization algorithm was included in that paper. Here, different to the findings of that study, a simpler approach is chosen, simply using a state dependant line segment of an initial and a target sliding manifold, then calculating the control signal based on the equivalent control law and saturation function defined. First let us derive the equivalent control in case of a constant sliding surface to illustrate the drawbacks of a constant sliding manifold.

2.1 Derivation of Control Law

Most commonly the sliding manifold is defined as

$$\sigma(\mathbf{x}) = \mathbf{c}^T \mathbf{x} = \lambda_1 \widetilde{\varphi}_{\mathrm{m}} + \widetilde{\Omega}_{\mathrm{m}}$$
 (8)

where, $c^T = [\lambda_1 1]$ is the vector defining the sliding manifold. Along the sliding manifold the error signal is null, and in case of continuous control the differential is also zero.

$$\mathbf{c}^T \dot{\mathbf{x}} = 0 \tag{9}$$

Therefore, by multiplying both sides of equation (3) by the sliding surface vector and solving for the control input, we can find the equivalent control law along the sliding surface in discrete time, derived in equation (10) we have:

$$u_{eq}(\mathbf{n}) = -(\mathbf{c}^T \mathbf{b})^{-1} \mathbf{c}^T \mathbf{A} (\mathbf{x} - \mathbf{x}^r)$$

= $s \cdot \varphi_{\mathbf{m}} + (k - \Theta_{\mathbf{m}} \lambda_1) \Omega_{\mathbf{m}}$ (10)

where n represents the *n*-th sampling time of the system, however for sake of brevity this will be neglected in the notation later on.

To handle the unknown nonlinear disturbance most commonly a switching-type control law is added to the equivalent control. In our case is a a saturation based control law:

$$u_{sw} = -M_e^{\text{max}} \cdot \text{sat}(\sigma(\mathbf{x})) \tag{11}$$

where, the sat($\sigma(\mathbf{x})$) function is defined as according to equation (12).

$$\operatorname{sat}(\sigma(\mathbf{x})) = \begin{cases} -1 & \text{if } \sigma(\mathbf{x}) < -\Delta \\ \frac{\sigma(\mathbf{x})}{\Delta} & \text{if } |\sigma(\mathbf{x})| < \Delta \\ 1 & \text{if } \sigma(\mathbf{x}) > \Delta \end{cases}$$
 (12)

Where, Δ is a design parameter. Thus the sliding phase control input can be written as:

$$u = u_{eq} + u_{sw} \tag{13}$$

It can be noticed, when all is written, that in this case the $-\Theta_{\rm m}\lambda_1\Omega_{\rm m}$ component of the equivalent control law impedes the maximum available torque output, especially in deep field weakening during reaching phase, thus restraining the control structure to output the maximal control signal. To minimize this problem one could say that tuning λ_1 sufficiently should be enough. However, this will be constly in dynamics near the equilibrium, or in an edge case, if $\lambda_1=0$, then the error signal $\sigma(\mathbf{x})=0$ will also hold, thus the control will not produce any torque reference. To attenuate this problem an adaptive sliding manifold is proposed.

2.2 Adaptive Sliding Manifold

The idea is to minimize the effect of this component of the control law while the motor is speeding up, and near the equilibrium we allow the full effect. Meaning, we wish the following characteristic for the parameter \mathbf{c}^T defined in equation (14).

$$\lim_{\substack{\widetilde{\varphi} \to 0 \\ \widetilde{\varphi} \to \text{inf}}} \mathbf{c}^{T}(\widetilde{\varphi}) = \mathbf{c}_{t}^{T}$$

$$\lim_{\substack{\widetilde{\varphi} \to \text{inf}}} \mathbf{c}^{T}(\widetilde{\varphi}) = \mathbf{c}_{ini}^{T}$$
(14)

In equation (14), the slope of the linear manifold has been made a function of the position error $\mathbf{c}^T(\tilde{\varphi})$, \mathbf{c}_{ini}^T is the initial slope and \mathbf{c}_t^T is the target slope.

However, if let us assume that the initial slope would be null $\mathbf{c}_{ini}^T = [0\ 1]$ then in many cases the initial error value $\sigma(\mathbf{x}) = 0$ would also hold. Therefore, the characteristics given in equation (14) are not sufficient alone. An initial offset is also to be set to ensure it. This can be imagined as an initial speed request that is to be reached, on the phase plane this would be represented as a constant speed offset, this characteristic is given in equation (15)

$$\lim_{\widetilde{\varphi} \to 0} \Delta_{\Omega}(\widetilde{\varphi}) = \Delta_{\Omega}^{t}$$

$$\lim_{\widetilde{\varphi} \to inf} \Delta_{\Omega}(\widetilde{\varphi}) = \Delta_{\Omega}^{ini}$$
(15)

where, $\Delta_{\Omega}(\widetilde{\varphi})$ is the speed offset value.

Then the line segment weighing function is also used here for the sliding manifold and the offset values resulting in the error signal

$$\sigma(\mathbf{x}) = \left(\delta(\tilde{\varphi})\mathbf{c}_{ini}^{T} + \left(1 - \delta(\tilde{\varphi})\right)\mathbf{c}_{t}^{T}\right)\mathbf{x} + \delta(\tilde{\varphi})\Delta_{\Omega}^{\text{ini}}\operatorname{sgn}(\tilde{\varphi})$$
(16)

as the target offset is $\Delta_{\Omega}^t=0$. Furthermore, where $\delta(\widetilde{\varphi})=\frac{1}{\Delta_{\widetilde{\varphi}}}|\widetilde{\varphi}(n)|-\frac{1}{\Delta_{\widetilde{\varphi_1}}}$. In this function, $\Delta_{\widetilde{\varphi_1}}$ and $\Delta_{\widetilde{\varphi}}$ are design parameters to set the initial and end position error of the line segment interpolation.

The control law is then equivalent in form to that of in equation (13), however the constant slope λ_1 is changed to weighted function:

$$\lambda_1 \to \left(\delta(\tilde{\varphi})\lambda_1^{\text{ini}} + \left(1 - \delta(\tilde{\varphi})\right)\lambda_1^{\text{t}}\right)$$
 (17)

With this are interpolation function is finished and are control law is defined along the phase plane. The simulation results are gathered in the following section.

3. SIMULATION RESULTS

In this section the simulation results are summarized. The simulations were built in Matlab/Simulink, the SW components were simulated in discrete time and the HW components were simulated in continuous time. The SW components ran with different sampling time, the DSMC had a sampling frequency of 1[kHz], while the current controller had a sampling frequency of 20[kHz]. In Table 1. the simulation parameters are gathered, which are relevant to the design of the sliding mode controller, such as maximum electric torque, and design parameters and driveline limitations. The parameters of IPMSM can be found in [8].

Table 1. Simulation Parameters

Name	Symbol	Value[unit]
Ini. Manifold	\mathbf{c}_{ini}^T	[50 1]
Tar. Manifold	\mathbf{c}_t^T	[0 1]
Ini. Offset	$\Delta_{\Omega}^{\mathrm{ini}}$	±800[rad/s]
Tar. Offset	$\Delta_{\Omega}^{ ext{t}}$	0[rad/s]
Weight fact.	$\Delta_{\widetilde{arphi}}$	59[rad]
Weight fact.	$\Delta_{\widetilde{arphi_1}}$	6[rad]
Boundary fact	Δ	150[-]
Act. Limit	$ \tilde{\varphi}(n) ^m$	110[rad]
Stiffness	S	0.063[Nm/rad]
Inertia	Θ_{m}	460e-6[kgm^2]
Damping	k	0.001[Nm/(rad/s)]
Max. Torque	$M_{\rm e}^{\rm max}$	12.73[Nm]
Max Hyst.	$M_{\eta}^{ m max}$	2[Nm]

The hysteresis hampering the system is shown in Fig. 2 Hysteresis characteristic of the electromechanical driveline Fig. 2, where it can be seen that the absolute value of it increases linearly according to the position of the system.

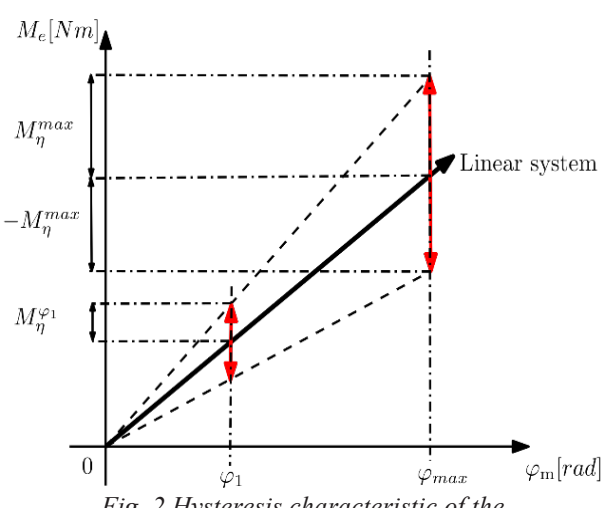


Fig. 2 Hysteresis characteristic of the electromechanical driveline

In Fig.3 the phase plane of the system is shown in case of a stepwise reference position change in both directions in succession of one-another.

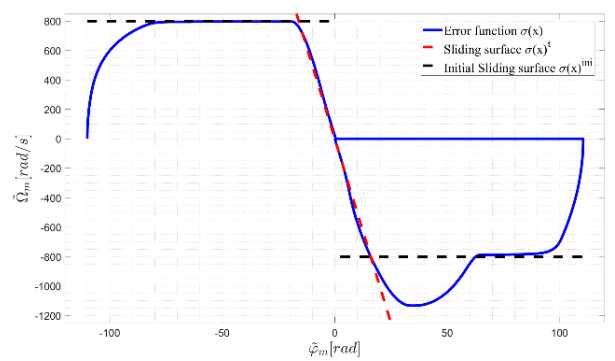


Fig.3. Phase plane of the electromechanical drive showing the initial sliding manifold, the target manifold, and the dynamical behavior of the system.

Initially, the state of the system follows the initial slope, then continuously converges to the target manifold in a stable fashion. There is no chattering along the system, but there are some oscillations in case of the reverse direction dynamics. In Fig. 4 the transient behavior of the controlled electromechanical system is presented.

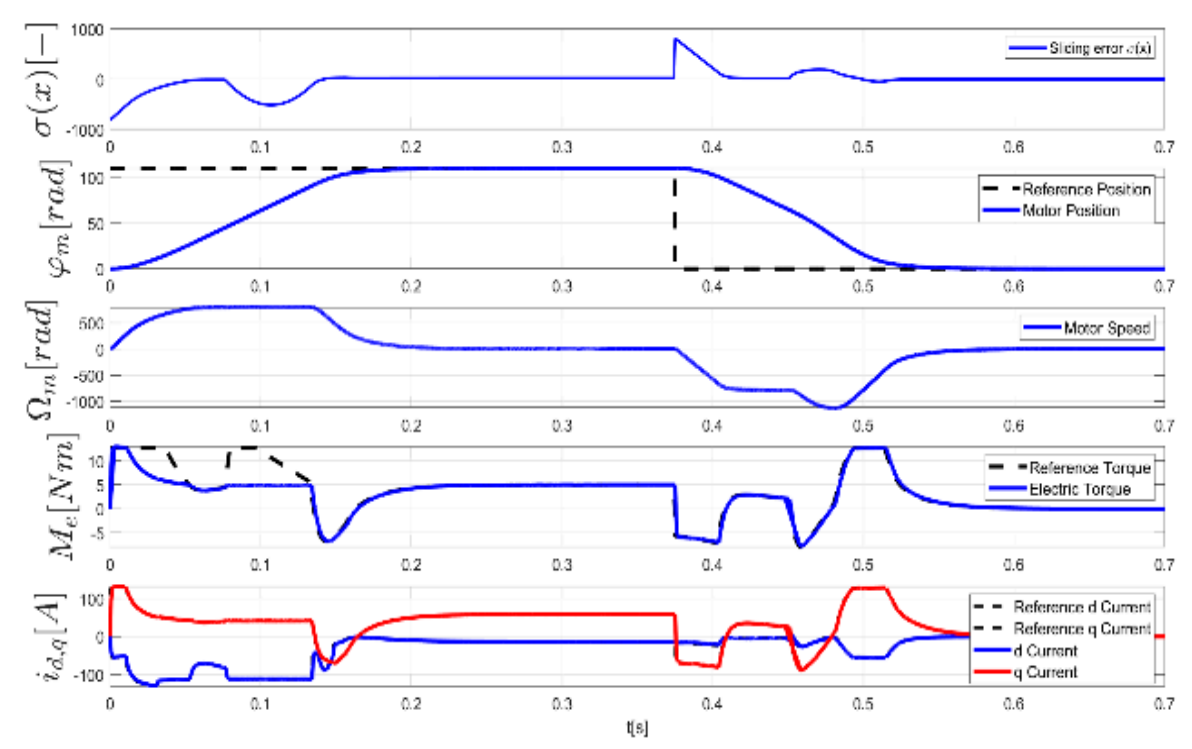


Fig. 4 Transient dynamics of the electromechanical driveline with adaptive sliding surface control.

The first plot of the figure shows the error signal $\sigma(x)$. Initially the error decreases, but as the sliding slope begins to change, the error increases, this was expected and stability was still maintained, but mathematical proof of stability should be provided in future work. The second subplot shows the position and reference position

of the motor. It can be seen that there is no chattering along the sliding mode. Furthermore, settling precision is high, as steady state error is approximately 0.5%. The third plot shows the speed of the machine, where in both directions it initially reaches the initial speed offset, then due to the energy provided by the spring in reverse

direction it can speed up even more. Subplot 4 shows the transient behaviour of the IPMSM. It can be seen that only in the initial portion of the dynamics does the realized electric torque follow the reference torque. This is due to the field-weakening characteristic of IPMSM motors. Above nominal speed the IPMSM cannot provide nominal torque, nonetheless, the reference generating algorithm always requests the maximum achievable torque in each working point. This is reinforced by subplot 5 where the lower level the lower level control efficiency is highlighted. It shows, that while the controller requests higher torque the reference generating algorithm only passed further realizable current references which resulted in smooth currents and good current following dynamics.

4. CONCLUSIONS AND FUTURE WORK

In conclusion the proposed simple adaptive sliding surface methodology coupled with the saturation function based switching function proved to be beneficial even in high hysteresis electromechanical systems according to simulation data. One main benefit is simplicity as only 3 design parameters are required, the other control parameters can be derived from motor parameters. Furthermore, the IPMSMs speed was indirectly limited in and the IPMSMs field weakening properties could be utilized effective with stable current control. The position error converged even in case of maximum dynamics in the $\pm 0.5\%$ range of the reference position, which is satisfactory in case of a high hysteresis system. Moreover, no chattering was experienced along the sliding manifold. In our future work we aim to also compensate the effects of hysteresis in case of low speed actuations with identification or observer methods. Also, in future works we aim to include measurement results.

5. REFERENCES

- [1] C. a. H.-P. D. a. V.-R. R. a. M.-M. D. Miguel-Espinar, "Review of Flux-Weakening Algorithms to Extend the Speed Range in Electric Vehicle Applications With Permanent Magnet Synchronous Machines," *IEEE Access*, pp. 22961-22981, 2023.
 - https://doi.org/10.1109/ACCESS.2023.3252360
- [2] X. a. F. Y. a. M. Z. Yu, "Terminal Sliding Mode Control – An Overview," *IEEE Open Journal of* the Industrial Electronics Society, pp. 36-52, 2021. https://doi.org/10.1109/OJIES.2020.3040412
- [3] A. Šabanovic, "Variable Structure Systems With Sliding Modes in Motion Control—A Survey," *IEEE Transactions on Industrial Informatics*, pp. 212-223, 2011. https://doi.org/10.1109/TII.2011.2123907
- [4] B. Wang, "On Discretized Sliding Mode Control Systems," *IFAC Proceedings Volumes*, pp. 13357-13361, 2011. https://doi.org/10.3182/20110828-6-IT-1002.03798
- [5] S. a. M. S. a. I. N. a. B. O. a. H. H. Amirkhani, "Fast terminal sliding mode tracking control of nonlinear uncertain mass–spring system with experimental verifications," *International Journal* of *Advanced Robotic Systems*, p., 2019. https://doi.org/10.1177/1729881419828176
- [6] J. a. Y. S. a. L. Y. a. K. W. Gil, "Super Twisting-Based Nonlinear Gain Sliding Mode Controller for Position Control of Permanent-Magnet Synchronous Motors," *IEEE Access*, pp. 142060-142070, 2021. https://doi.org/10.1109/ACCESS.2021.3121127
- [7] K. a. L. J. a. K. M. a. Y. K. Kim, "Adaptive Sliding Mode Control of Rack Position Tracking System for Steer-by-Wire Vehicles," *IEEE Access*, pp. 163483-163500, 2020. https://doi.org/10.1109/ACCESS.2020.3021038
- [8] P. a. T.-K. T. Stumpf, "Optimal Searching-Based Reference Current Computation Algorithm for IPMSM Drives Considering Iron Loss," *Actuators*, p., 2024. https://doi.org/10.3390/act13080321
- [9] M. a. A. A. A. H. a. Q. Z. a. T. T. a. B. F. Hinkkanen, "Current Control for Synchronous Motor Drives: Direct Discrete-Time Pole-Placement Design," *IEEE Transactions on Industry Applications*, pp. 1530-1541, 2016. https://doi.org/10.1109/TIA.2015.2495288
- [10] P. Hušek, "Adaptive sliding mode control with moving sliding surface," *Applied Soft Computing*, pp. 178-183, 2016. https://doi.org/10.1016/j.asoc.2016.01.009